2022 International Conference on Rehabilitation Robotics (ICORR)
25-29 July, 2022, Rotterdam, The Netherlands

2022 International Conference on Rehabilitation Robotics (ICORR) | 978-1-6654-8829-7/22/$31.00 ©2022 IEEE | DOI: 10.1109/ICORR55369.2022.9896517

Neural data-driven model of spinal excitability changes induced by transcutaneous electrical stimulation in spinal cord injury subjects

R. Ornelas Kobayashi, A. Gogeascoechea, L. Joseph Tomy, E. Van Asseldonk, M. Sartori

Abstract— **The efficacy of trans-spinal direct current stimulation (tsDCS) as neurorehabilitation technology remains sub-optimal, partly due to the variability introduced by subject-specific neurophysiological features and stimulation conditions (*e.g.* electrode placement, stimulating amplitude, polarity, etc.) Hence, current therapies apply tsDCS in an open-loop fashion, resulting in a lack of standardized protocols for controlling elicited neuronal adaptations in closed-loop. Through the combination of high-density electromyogram (HD-EMG) decomposition, biophysical neuronal modelling and metaheuristic optimization, this work presents a novel neural data-driven framework for estimating subject-specific features and quantifying acute neuronal adaptations elicited by tsDCS on incomplete spinal cord injury subjects. This approach consists of calibrating the anatomical parameters *(e.g.* soma diameter) of *in silico* α-motoneuron (MN) models for firing similarly to *in vivo* MNs decoded from HD-EMG. Assuming that cathodal-tsDCS elicits excitability changes in the MN pool, while preserving their anatomical parameters, optimization of an excitability gain common to the entire pool was performed to minimize discrepancies in firing rate and recruitment time between *in vivo* and *in silico* MNs after cathodal-tsDCS. This quantification of excitability changes on MN models calibrated in a person specific way enables closing the loop with neuro-modulation devices to tailor neurorehabilitation therapies.**

Clinical Relevance— **This framework addresses a key limitation in non-invasive neuro-modulative technologies via a novel model-assisted framework that enables quantifying acute excitability changes induced on a person-specific *in silico* MN pool calibrated using *in vivo* neural data. This will enable the development of advanced controllers for modulating targeted neuronal adaptations in closed-loop.**

I. Introduction

Spinal cord injury (SCI) may result from a traumatic injury disrupting the communication between (supra) spinal structures and the spinal neurons below the injury site. Such disruption results in structural changes and alterations of spinal neuron excitability [1], which may lead to chronic pain [2], sensory-motor impairment [3] and spasticity [4]. Current non-invasive neurorehabilitation technologies aiming at restoring the sensory-motor function include physical activity, cell therapy, pharmacological drugs and electrical stimulation of the spine [5], with the latter gaining increasing interest over the last decade. Trans-spinal direct current stimulation (tsDCS) consists in delivering weak electrical currents into the spinal cord through surface electrodes placed over the skin. TsDCS has the potential of modulating plasticity in the spinal circuitry [6] and promote long-lasting adaptations after stimulation offset, when integrated in activity-based rehabilitation programs [7]. Although the exact mechanism of interaction remains unclear, tsDCS is known to induce changes in the excitability and rhythmic firing of α-motoneurons (MNs) [8]–[10] depending on the polarity of the stimulating current (*i.e.,* anodal facilitates and cathodal depresses MN firing). Moreover, the non-invasive nature of tsDCS makes it a widely used alternative in the treatment of spasticity [11] and chronic tetraplegia [12]. However, stimulation protocols and neural responses to tsDCS vary largely across individuals, partly due to subject-specific neurophysiological features, electrodes placement and lesion-specific neuropathology. As a result, current tsDCS therapies follow highly empirical approaches, sometimes even failing at eliciting any response [13]. Therefore, there is a need for developing standardized protocols and quantitative tools for targeting and controlling elicited neuronal adaptations.

In this context, the ability of measuring the firing properties of *in vivo* MNs, which represent the final common pathway of the central nervous system, becomes crucial to quantify the acute and long term adaptations elicited by tsDCS. In previous work, we provided evidence that the *in vivo* common synaptic input (CSI) received by the MN pool could be derived from motor unit spike trains decoded via high-density electromyogram (HD-EMG) decomposition and be subsequently used as reference for the metaheuristic optimization of geometrical and electrical parameters of biophysical MN models [14]. This approach enabled *in silico* MN models to fire similarly as *in vivo* MNs.

In this work, we present a novel neural data-driven framework where *in silico* MN models are calibrated in a person specific way for quantifying MN properties on SCI subjects, and estimating acute tsDCS-induced adaptations on SCI subjects. Preliminary results demonstrate that this approach is capable

*This work was funded by the European Research Council (ERC) under the European Union's Horizon 2020 research and innovation program as part of the ERC Starting Grant INTERACT (No. 803035).

R. Ornelas Kobayashi. A. Gogeascoechea, L. Joseph Tommy, E. Van Asseldonk and M. Sartori are with the Department of Biomechanical Engineering, University of Twente, Netherlands (email: r.e.ornelaskobayashi@utwente.nl).

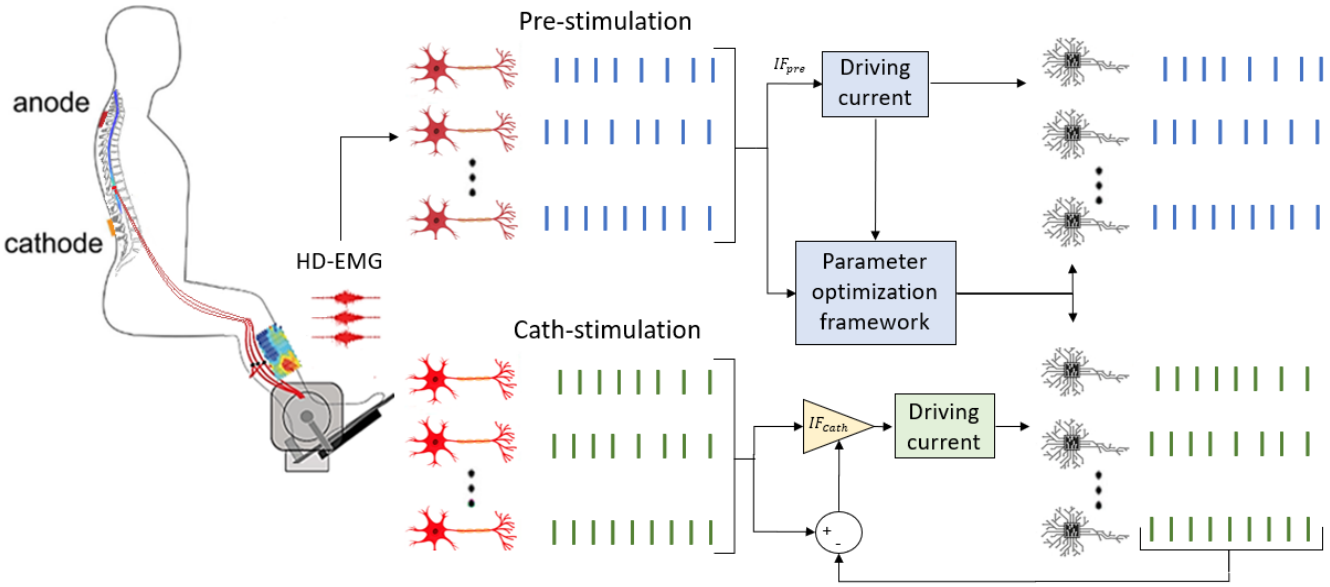

Figure 1. Overview of the neural data-driven model for quantifying excitability changes: *In-vivo* motoneurons (MNs) spike trains are decomposed from high-density electromyogram recordings pre- (blue) and post cathodal- (red) trans-spinal direct current stimulation (tsDCS). Net MN pool discharge rate (NDR) is estimated from decoded MN spikes, and the corresponding common synaptic current is derived from the product between the respective NDR and the excitability constant. The initial excitability constant IF_{Pre} is determined by fitting the theoretical MN diameter range to the experimental recruitment times. MN model optimization is then performed for every decoded MN to reproduce the same firing pattern as pre-tsDCS *in vivo* MNs. Subsequently, tsDCS-induced changes were quantified by optimizing post cathodal-tsDCS excitability constant (IF_{cath}) to minimize discharge rate and recruitment time root mean squared error between *in silico* MN models and post cathodal-tsDCS *in vivo* MNs.

of capturing changes in the MN pool excitability, which opens new avenues for the development of closed-loop non-invasive neurorehabilitation technologies, where stimulation protocols and parameters can be automatically adjusted for the optimal modulation of a target neuronal adaptation.

II. METHODS

A. Participant description

The subject included in this study was a 62 years old male with chronic incomplete SCI at the level of the 4th cervical vertebrae [15]. According to the American spinal injury association, participant had a SCI impairment scale (AIS) D, walking index > 1 and independence measure > 30. Before the experiment, the subjects signed a written informed consent and all study procedures were approved by the local Ethics Committee of Twente (METC Twente, reference number: NL49561.044.14 / P14-22).

B. Experimental procedure

Throughout the experiment, the participant was seated on a medical chair and tightly strapped by built-in racing belts to avoid any trunk movement. Supported by a solid frame with Velcro straps, the right leg was fixed to keep hip, knee and ankle joint angles of 90°. Ankle plantar-flexion torque was measured using a force plate (Advanced Mechanical Technology, Inc., Watertown, USA), while HD-EMG was recorded from the Soleus muscle using an 8x8 electrode grid and TMSi Refa multichannel amplifier (TMS International B.V., Oldenzaal, The Netherlands) at a sampling frequency of 2,048 Hz. The maximum voluntary contraction (MVC) was determined as the highest plantarflexion force achieved by the subject out of three trials (spaced by a 1-2 min resting time) applying as much force as possible during 5s.

As previously described [15], the participa received cathodal and sham tsDCS, where sham was the control condition. In both cases, the active electrode was centered between 11th and 12th thoracic vertebras, and the ground electrode placed over the right shoulder. Stimulation was applied via a custom-build stimulator (TMS International B.V., Oldenzaal, The Netherlands) while performing a force tracking task of sinusoidal waves with mean amplitude of 5% to 10% MVC.

To assess the effect of tsDCS, three conditions were analyzed: before stimulation (pre-tsDCS), immediately after sham (sham-tsDCS) and after cathodal stimulation (cathodal-tsDCS) [15]. For each condition, torque and HD-EMG were recorded from the subject following a ramp force profile of 20%MVC, with a 25s plateau and a speed of 2.5MVC/s during both ascending and descending parts. HD-EMG data was then decomposed into individual spike trains using convolution kernel compensation [16]. Each spike train was defined as a binary vector where 1 represented a spike event and 0 meant no firing activity.

C. Biophysical motoneuron model

MN models were implemented as single-compartment conductance-based models (Fig 2). The included ionic channels were sodium (g_{Na}), slow (g_{Ks}) and fast potassium (g_{Kf}), which were shown to enable reproducing experimental neuronal behavior [17]. Equations (1) and (2) describe the MN model, where E_{Na} and E_K correspond to the reverse potentials

of sodium and potassium, respectively, Rm is the membrane resistance, Cm the capacitance, and D_s the soma diameter. As proposed by Cisi and Kohn [17], the voltage-dependent rate constants m, n and h were computed according to a pulse-based approach [18] that maximizes computational efficiency. Instead of solving the set of differential equations described by Hodgkin and Huxley [19], the pulse-based model emulates the action potential as a threshold-dependent rectangular pulse, during which the dynamics of each ionic channels are given exclusively by defined parameters beta (β) and alpha (α) [18].

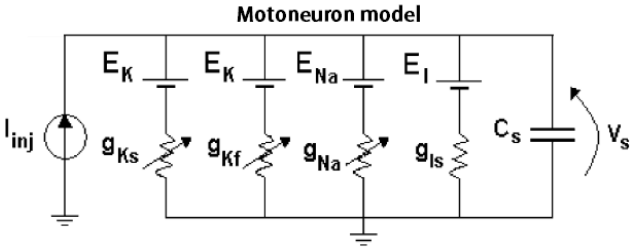

Figure 2. Electrical circuit of the single-compartment motoneuron model depicting the reverse potentials and conductances of all the included ionic channels (adapted from [17])

$$I_{ion} = g_{Na}m^3h(E_{Na} - V_m) + g_{Kf}n^4(E_K - V_m) + g_{Ks}q^2(E_K - V_m) \quad (1)$$

$$V_m = \left(\frac{\pi {D_s}^2}{R_m}(E_L - V_m) + I_{ion} + I_{inj}\right)\left(\frac{dt}{\pi C_m {D_s}^2}\right) \quad (2)$$

D. Parameter optimization framework

Previous work [14] demonstrated that, driven by an experimentally derived input current, multiple-objective optimization of D_s and β_{ks} minimizes the error between experimental and simulated MN recruitment times and firing patterns, respectively. In order to improve computational time and sampling of the optimal pareto space [20], the hereby proposed MN model optimization framework implemented genetic algorithm (GA) for two consecutive single-objective optimization problems. First, recruitment time error (3) was minimized by optimizing only D_s. Then, the initial GA population of β_{Ks} and α_{Ks} was created based on their corresponding MN-type values [21], and second optimization was executed adjusting both β_{Ks} and α_{Ks} to minimize the frequency-corrected spike match error (4) [22]. In both cases, GA was set for a population size of 200, elite percentage of 10% and 70% cross-over with a function tolerance of 0.01.

$$2\left|\frac{\text{spikes}_\text{e}(i) - \text{spikes}_\text{m}(i)}{\text{spikes}_\text{e}(i)}\right|_{i=1} \quad (3)$$

$$2\left|\frac{f_e - f_m}{f_e}\right| - \frac{2}{1 - 2\delta f_e}\left(\frac{N_c - 2\delta f_e N_e}{N_e + N_m}\right) \quad (4)$$

Where f_e and f_m are mean firing rate, N_e and N_m number of spikes, and $spikes_e$ and $spikes_m$ the spike trains of experimental and model MNs, respectively. N_c is number of coincident spikes within a time window of δ = 2ms [22].

Parameter optimization was performed by driving the MN models with the common synaptic input derived from the pre-tsDCS condition current (see section II.E). To ensure physiologically realistic solutions throughout optimizations, D_s lower and upper boundaries were set to 20 and 200µm [23], respectively, whereas the boundaries of β_{Ks} and α_{Ks}, as well as all the non-optimized parameters, were kept the same as defined by Elias and Kohn [24].

E. Common input current estimation

The main challenge for fitting neuronal models to *in vivo* neural spike trains is the measuring of the input current received by the MNs. Theoretical findings [25], however, suggest that the low-frequency components of the common synaptic input (CSI) received by the MN pool are linearly transformed into the neural drive to muscle (ND), which represents the MN pool net discharge rate (NDR), and can be estimated from experimental spike trains [26]. Consequently, we propose the non-invasive estimation of the *in vivo* CSI as the experimentally-derived ND multiplied by an excitability constant. Given the linear relationship between input current and MN firing frequency below 40Hz [27], [28], we defined this excitability constant as the current-frequency (I-F) slope between NDR (in Hertz) and CSI amplitude (in pA). To estimate pre-tsDCS NDR, we created a cumulative spike train (CST) summing the individual spike trains of all pre-tsDCS decoded MNs. The instantaneous CST discharge rate was calculated according to (5), where t_n represents the discharge time of the n^{th} spike in the CST. The resulting signal was filtered by a moving average window of 500 samples [26] and normalized to have the same mean discharge rate as the averaged mean discharge rate of all individual MN comprising the CST.

$$DR_n = \frac{1}{t_n - t_{n-1}} \quad (5)$$

The pre-tsDCS excitability constant (IF_{pre}) was defined as the optimal I-F slope that minimizes the recruitment error (3) between: a) earliest recruited experimental MN and simulated MN with D_s = 20µm, and b) latest recruited experimental MN and simulated MN with D_s = 200µm. GA was executed as a multi-objective optimization problem where both a) and b) were optimized simultaneously and independently from each other to find the optimal pareto front for both error functions. Afterwards, Gray relational analysis (GRA) [29] was applied to automatically select the best IF_{pre} solution from the optimal pareto set. Lastly, the product of NDR and best IF_{pre} was computed to obtain the CSI that drives MNs models during parameter optimization (see section II.D).

F. Excitability changes induced by tsDCS

Excitability changes in the MN pool were quantified by estimating the cathodal-induced excitability constant (IF_{Cath}). The value of IF_{Cath} was determined using GA multi-objective optimization to minimize the root mean squared error (RMSE) between a) mean discharge rates and b)

recruitment times of optimized MN models and *in vivo* MNs during cathodal-tsDCS. For this, optimized MN models were driven by the CSI derived from the cathodal-tsDCS condition (see section II.E). GRA was applied to the resulting optimal pareto front in order to determine the best IF_{Cath} that equally minimizes the RMSE of both mean discharge rates and recruitment times. For control, the same process was performed on the sham-tsDCS condition to determine the corresponding IF_{Sham}.

III. RESULTS

The optimal pareto set of IF_{pre} and IF_{Cath} are shown in Fig 3, and Fig 4, respectively, with the best solution determined by GRA highlighted in red. The IF_{pre} value of 0.2018 achieved a relative recruitment error of 0.129s for the last recruited MN, and 0.104s for the first MN. The optimized parameters D_s, β_{Ks} and α_{Ks} of each of the nine *in vivo* identified MNs (pre-tsDCS) are shown in Fig 5, with their corresponding distributions. Noticeably, the proportion of small diameter MNs is substantially larger than that of high diameter MNs.

The optimal $IF_{Cath} = 0.253$ achieved recruitment time and mean discharge rate RMSEs of 0.083 and 2.48, respectively.

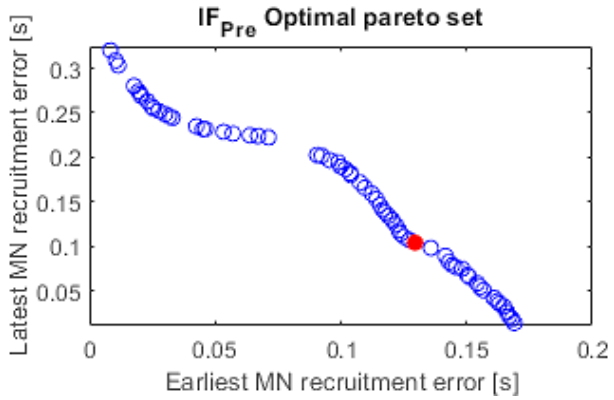

Figure 3. Optimal pareto front highlighting in red GRA's best solution for minimizing recruitment error of both earliest and latest recruited MNs.

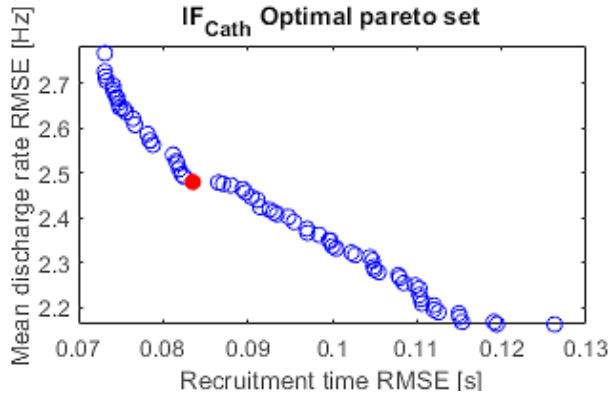

Figure 4. Optimal pareto front highlighting in red GRA's best solution for minimizing recruitment time and mean discharge rate RMSE between all optimized MN models and *in vivo* MNs during cathodal-tsDCS.

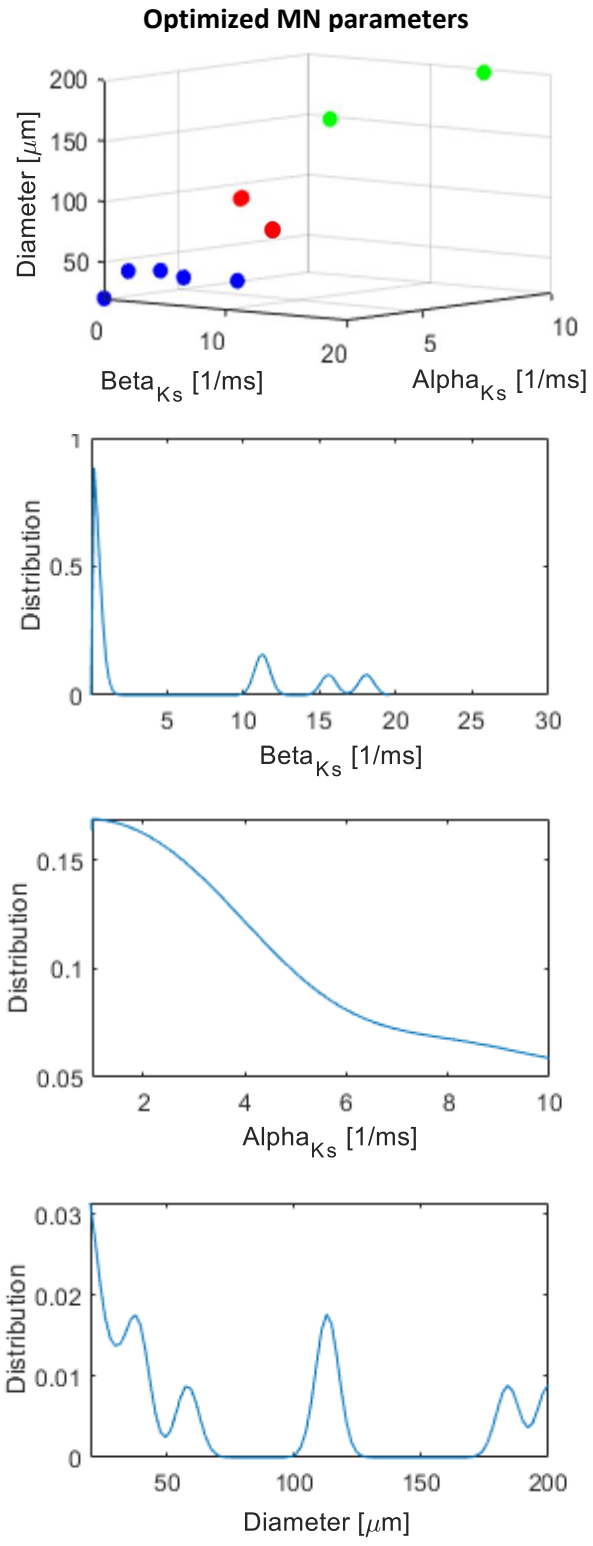

Figure 5. MN parameters as determined by the optimization framework. The three-dimensional plot on top shows each *in vivo* decoded MN as a dot characterized by its corresponding set of parameters D_s, β_{Ks} and α_{Ks}. For visualization, MNs within a diameter range 20 and 40μm are color coded in blue, red between 40 and 150 μm, and larger diameter values in green. Additionally, this figure shows the identified distribution of each parameter within the MN pool.

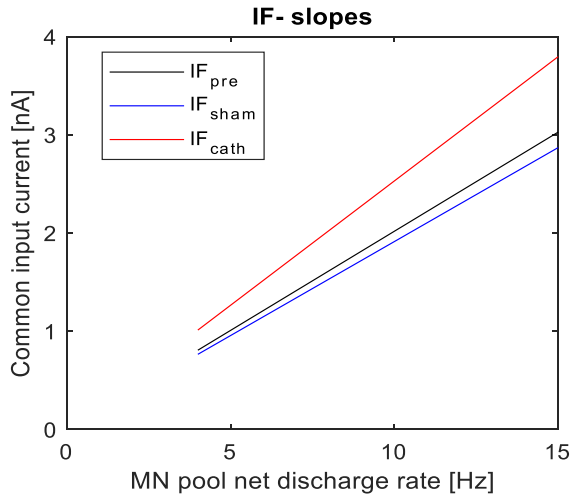

Figure 6. Optimal I-F slopes determined for each condition: no-stimulation (black), sham (blue) and cathodal-stimulation (red)

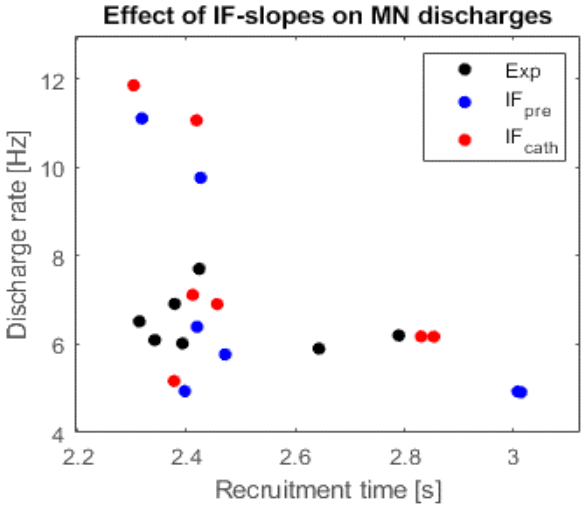

Figure 7. MNs firing characteristics during cathodal-tsDCS. *In vivo* MNs are depicted in black, simulated MNs before excitability constant optimization (IF_{pre}) in blue, and after (IF_{Cath}) in red.

Figure 8. Absolute mean discharge rate and recruitment time error between cathodal-tsDCS *in vivo* and model MNs before optimization of excitability constant (IF_{pre}) and after optimization (IF_{Cath}).

While the respective RMSE values achieved by the optimal $IF_{Sham} = 0.1913$ were 0.165 and 2.47. The contrast between all three slopes is shown in Fig 6. IF_{Sham} was remarkably similar to IF_{pre}, whereas IF_{cath} resulted in a considerably larger slope. Fig 7 depicts the average discharge rate and recruitment time of the seven *in vivo* MNs identified from the cathodal-tsDCS condition, together with the corresponding *in silico* MNs driven by the CSI derived using IF_{pre} and IF_{cath}. As observed, the change in I-F slope enables simulated MNs to better replicate the firing characteristics of the post-tsDCS experimental MNs. Absolute errors in discharge rate and recruitment are summarized in Fig 8.

IV. DISCUSSION

We proposed a subject-specific neural data-driven modelling framework for estimating MN properties and acute tsDCS-induced adaptations in SCI-individuals. Model estimations of excitability changes due to cathodal tsDCS are seen in Fig 6, where the steeper value of IF_{Cath}, in comparison to IF_{Sham} and IF_{Pre}, implies that an increased input current is necessary for a same NDR. This supports experimental evidence of cathodal tsDCS depressing MNs excitability [10]. As shown in Fig 8, IF_{Cath} improves both mean discharge rate and recruitment time error in comparison to IF_{Pre}. However, differences in MNs firing characteristics persist after optimization, suggesting that other mechanisms such as post-activation depression [30] and alterations in common synaptic input [15] may need to be included to achieve a better fit. Moreover, while IF_{Cath} decreased the mean firing frequency error, it also increased the variability in discharges. This may be an effect of cathodal tsDCS [15], although further studies in this direction are necessary, which may look into the inclusion of additional ionic channels in the MN models to better capture the firing behaviors of *in vivo* MNs.

To match *in vivo* and *in silico* MNs recruitment time, parameter optimization assumed a soma diameter range of 20 to 200µm. Although this range was taken from cadaver studies [23], discrepancies in morphology are to be expected, particularly after SCI [31] and neurogenerative diseases [32]. Furthermore, to estimate IF_{Pre}, the framework assumes that the earliest recruited MN was that of smallest diameter (20 µm), while the latest recruited had the largest diameter (200 µm). To evaluate the impact of such fixed diameter ranges and test whether these methods and results generalize to more individuals, future work should focus on the parameter distributions and excitability constants of a larger number of SCI and healthy subjects. Since this work presented preliminary results from only one SCI subject, the study lacks statistical power. However, it stands as a demonstration of the distinctive role of the I-F slope for reducing discrepancies in the firing characteristics of MNs after cathodal stimulation within a same subject. Furthermore, future works should also assess H-reflex before and after stimulation to validate our estimation of IF_{Pre}, IF_{Sham} and IF_{Cath}.

Lastly, this approach inherits an intrinsic limitations of HD-EMG decomposition [33]: larger motor units (producing

action potentials of higher amplitude) overshadow smaller units, thus limiting the total number of decomposed MNs and neglecting the contribution of earlies recruited MNs, further adding to the issue of a fixed diameter range. Moreover, as the number of identified MNs may vary across tasks, a robust algorithm for tracking motor units across conditions may be necessary to properly link *in silico* and *in vivo* MNs.

V. Conclusion

This work provides evidence of the ability of this neural data-driven framework for non-invasively estimating MN properties of SCI subjects, and quantifying tsDCS-induced excitability changes in the MN pool. This opens new avenues for the development of model-based closed-loop controllers for neuro-modulation technologies.

References

[1] s. M. Elbasiouny, d. Moroz, m. M. Bakr, and v. K. Mushahwar, "management of spasticity after spinal cord injury: current techniques and future directions," *neurorehabil. Neural repair*, vol. 24, no. 1, pp. 23–33, 2010, doi: 10.1177/1545968309343213.

[2] s. Störmer *et al.*, "chronic pain/dysaesthesiae in spinal cord injury patients: results of a multicentre study," *spinal cord*, vol. 35, no. 7, pp. 446–455, 1997, doi: 10.1038/sj.sc.3100411.

[3] m. R. Dimitrijevic, s. M. Danner, and w. Mayr, "neurocontrol of movement in humans with spinal cord injury," *artif. Organs*, vol. 39, no. 10, pp. 823–833, 2015, doi: 10.1111/aor.12614.

[4] f. Biering-sørensen, j. B. Nielsen, and k. Klinge, "spasticity-assessment: a review," *spinal cord*, vol. 44, no. 12, pp. 708–722, 2006, doi: 10.1038/sj.sc.3101928.

[5] c. Pizzolato *et al.*, "non-invasive approaches to functional recovery after spinal cord injury : therapeutic targets and multimodal device interventions," *exp. Neurol.*, vol. 339, no. January, p. 113612, 2021, doi: 10.1016/j.expneurol.2021.113612.

[6] t. Yamaguchi, s. Fujimoto, y. Otaka, and s. Tanaka, "effects of transcutaneous spinal dc stimulation on plasticity of the spinal circuits and corticospinal tracts in humans," *int. Ieee/embs conf. Neural eng. Ner*, pp. 275–278, 2013, doi: 10.1109/ner.2013.6695925.

[7] f. Cogiamanian *et al.*, "transcutaneous spinal direct current stimulation," vol. 3, no. July, pp. 1–5, 2012, doi: 10.3389/fpsyt.2012.00063.

[8] t. Bocci, b. Vannini, a. Torzini, and a. Mazzatenta, "cathodal transcutaneous spinal direct current stimulation (tsdcs) improves motor unit recruitment in healthy subjects," *neurosci. Lett.*, pp. 1–5, 2014, doi: 10.1016/j.neulet.2014.06.037.

[9] w. Song, d. Q. Truong, m. Bikson, and j. H. Martin, "transspinal direct current stimulation immediately modifies motor cortex sensorimotor maps," *j. Neurophysiol.*, vol. 113, no. 7, pp. 2801–2811, 2015, doi: 10.1152/jn.00784.2014.

[10] m. Bączyk, h. Drzymała-celichowska, w. Mrówczyński, and p. Krutki, "motoneuron firing properties are modified by trans-spinal direct current stimulation in rats," *j. Appl. Physiol.*, vol. 126, no. 5, pp. 1232–1241, 2019, doi: 10.1152/japplphysiol.00803.2018.

[11] u. S. Hofstoetter, w. B. Mckay, k. E. Tansey, w. Mayr, h. Kern, and k. Minassian, "modification of spasticity by transcutaneous spinal cord stimulation in individuals with incomplete spinal cord injury," *j. Spinal cord med.*, vol. 37, no. 2, pp. 202–211, 2014, doi: 10.1179/2045772313y.0000000149.

[12] f. Inanici, s. Samejima, p. Gad, v. R. Edgerton, c. P. Hofstetter, and c. T. Moritz, "transcutaneous electrical spinal stimulation promotes long-term recovery of upper extremity function in chronic tetraplegia," *ieee trans. Neural syst. Rehabil. Eng.*, vol. 26, no. 6, 2018, doi: 10.1109/tnsre.2018.2834339.

[13] m. Pereira, s. R. Fernandes, p. C. Miranda, and m. De carvalho, "neuromodulation of lower limb motor responses with transcutaneous lumbar spinal cord direct current stimulation," *clin. Neurophysiol.*, vol. 129, no. 9, pp. 1999–2009, 2018, doi: 10.1016/j.clinph.2018.07.002.

[14] r. O. Kobayashi, a. Gogeascoechea, j. Buitenweg, u. Yavuz, and m. Sartori, "optimization framework for the model-based estimation of in vivo α -motoneuron properties in the intact human," no. 803035, pp. 6133–6136, 2021.

[15] a. Gogeascoechea, a. Kuck, e. Van asseldonk, f. Negro, j. Buitenweg, and m. Sartori, "interfacing with alpha motor neurons in spinal cord injury patients receiving trans-spinal electrical stimulation," *front. Neurol.*, vol. 11, no. June, pp. 1–12, 2020, doi: 10.3389/fneur.2020.00493.

[16] a. Holobar, "accurate identification of motor unit discharge patterns from high-density surface emg and validation with a novel signal-based performance metric," 2014, doi: 10.1088/1741-2560/11/1/016008.

[17] r. R. L. Cisi and a. F. Kohn, "simulation system of spinal cord motor nuclei and associated nerves and muscles , in a web-based architecture," pp. 520–542, 2008, doi: 10.1007/s10827-008-0092-8.

[18] a. Destexhe, "conductance-based integrate-and-fire models," *neural comput.*, vol. 9, no. 9, pp. 503–514, 1997, doi: 10.1162/neco.1997.9.3.503.

[19] a. L. Hodgkin and a. F. Huxley, "a quantitative description of membrane current and its application to conduction and excitation in nerve," *j. Physiol.*, vol. 117, pp. 500–544, 1952.

[20] g. Guariso, "improving the performance of multiobjective genetic algorithms : an elitism-based approach," 2020, doi: 10.3390/info11120587.

[21] r. N. Watanabe, f. H. Magalhães, l. A. Elias, v. M. Chaud, e. M. Mello, and a. F. Kohn, "influences of premotoneuronal command statistics on the scaling of motor output variability during isometric plantar flexion," *j. Neurophysiol.*, vol. 110, no. 11, pp. 2592–2606, 2013, doi: 10.1152/jn.00073.2013.

[22] c. Clopath, r. Jolivet, a. Rauch, h. R. Lüscher, and w. Gerstner, "predicting neuronal activity with simple models of the threshold type: adaptive exponential integrate-and-fire model with two compartments," *neurocomputing*, vol. 70, no. 10–12, pp. 1668–1673, 2007, doi: 10.1016/j.neucom.2006.10.047.

[23] a. Caillet, a. T. M. Phillips, d. Farina, and l. Modenese, "mathematical relationships between motoneuron properties derived by empirical data analysis : size determines all motoneuron properties," pp. 1–27, 2021.

[24] f. Kohn and l. Abdala, "individual and collective properties of computationally efficient motoneuron models of types s and f with active dendrites," vol. 99, pp. 521–533, 2013, doi: 10.1016/j.neucom.2012.06.038.

[25] d. Farina and f. Negro, "common synaptic input to motor neurons , motor unit synchronization , and force control," no. 5, pp. 23–33, 2015.

[26] m. Sartori, u. Ş. Yavuz, and d. Farina, "in vivo neuromechanics : decoding causal motor neuron behavior with resulting musculoskeletal function," no. September, pp. 1–14, 2017, doi: 10.1038/s41598-017-13766-6.

[27] r. Granit, d. Kernell, and g. K. Shortess, "quantitative aspects of repetitive firing of mammalian motoneurones, caused by injected currents," *j. Physiol.*, pp. 911–931, 1963.

[28] k. D. B. Powers and m. D. Binder, "experimental evaluation of input-output motoneuron discharge models of," vol. 75, no. 1, pp. 367–379, 2018.

[29] z. Wang and g. P. Rangaiah, "application and analysis of methods for selecting an optimal solution from the pareto-optimal front obtained by multiobjective optimization," *ind. Eng. Chem. Res.*, vol. 56, no. 2, pp. 560–574, 2017, doi: 10.1021/acs.iecr.6b03453.

[30] t. Winkler, p. Hering, and a. Straube, "spinal dc stimulation in humans modulates post-activation depression of the h-reflex depending on current polarity," *clin. Neurophysiol.*, vol. 121, no. 6, pp. 957–961, 2010, doi: 10.1016/j.clinph.2010.01.014.

[31] p. Bose, r. Parmer, p. J. Reier, and f. J. Thompson, "morphological changes of the soleus motoneuron pool in chronic midthoracic contused rats," *exp. Neurol.*, vol. 191, no. 1, pp. 13–23, 2005, doi: 10.1016/j.expneurol.2004.08.028.

[32] s. S. Dukkipati, t. L. Garrett, and s. M. Elbasiouny, "the vulnerability of spinal motoneurons and soma size plasticity in a mouse model of amyotrophic lateral sclerosis," vol. 9, pp. 1723–1745, 2018, doi: 10.1113/jp275498.

[33] a. G. Hernandez, r. O. Kobayashi, u. S. Yavuz, and m. Sartori, "identification of motor unit twitch properties in the intact human in vivo," *proc. Annu. Int. Conf. Ieee eng. Med. Biol. Soc. Embs*, no. 803035, pp. 6310–6313, 2021, doi: 10.1109/embc46164.2021.9630328.